Hindawi
Advances in Civil Engineering
Volume 2022, Article ID 3386025, 10 pages
https://doi.org/10.1155/2022/3386025

Research Article

Effects of the Particle Shape and Size on the Single-Particle Breakage Strength

Yun Qing[1,2], **Zhenfeng Qiu**[1,2], **Yi Tang**[1], **Wenjie Deng**[3], **Xujin Zhang**[1], **Jilun Miu**[1] and **Shaoxian Song**[4]

[1]*Key Laboratory of Hydraulic and Waterway Engineering of Ministry of Education, Chongqing Jiaotong University, Chongqing 400074, China*
[2]*Engineering Research Center of Diagnosis Technology and Instruments of Hydro-Construction, Chongqing Jiaotong University, 66 Xuefu Road, Nan'an District, Chongqing 400074, China*
[3]*Chongqing Chuandongnan Survey & Design Institute Co., Ltd, Chongqing 400038, China*
[4]*Chongqing Municipal Design and Research Institute Co., Ltd, Chongqing 400015, China*

Correspondence should be addressed to Zhenfeng Qiu; 429158988@qq.com

Received 17 June 2022; Revised 5 October 2022; Accepted 6 October 2022; Published 1 December 2022

Academic Editor: Valeria Vignali

The strength and deformation of a soil foundation are related to the strength of each particle. Maybe the shape affects the strength of a particle. In this study, single-particle breakage tests were conducted on limestone particles of different sizes to analyze the influence of limestone particle shapes on the particle crushing strength. The results showed that 90 percent of limestone particle shapes were oblate spherical, subspherical, and long spherical particles randomly selected from the soil foundation. The single-particle breakage test results showed that the characteristic stress of limestone particles increases with the increased particle size. The crushing strength of limestone particles increased with the increase in particle size. There was a significant size effect on the single-particle compressive strength. The relationship between the characteristic strength and the particle size can be fitted by a power exponential formulation of four types of limestone particle shapes. The more irregular the particle shape, the smaller the Weibull modulus (m) and the power index and the more obvious the particle strength size effect.

1. Introduction

Granular materials, such as sands, rock-fill, and coarse-grained soil, are widely used in ports and wharf fills, dams, and foundation works. The strength and deformation of the filler are important indicators that threaten the safety of the structure. The mechanical properties of the filler are affected by many factors, including particle composition, mechanical properties of particles, shape, size, and roughness of compositions [1–5]. Brzesowsky et al. [6] investigated the adaptability of the micromechanical model for single-particle compression failure based on Hertz fracture mechanics and linear elastic fracture mechanics. Frossard et al. [7] proposed a novel method to evaluate the shear strength of coarse-grained soil based on the size effect of particle strength from the perspective of fracture mechanics. Wang et al. [8] and Huang et al. [9] showed that the relationship between the cumulative survival probability and the crushing stress of particles follows the Weibull distribution. Xu et al. [10] and Mi and Chi [11] established the correlation between the particle crushing strength and particle size based on the fractal model and the logistic equation. Li et al. [12] postulated that the size effect differs from normal contact force and anisotropy at the microscopic level, causing a difference in peak strength. Huang et al. [13] performed a simulation using the particle flow code and found that particle size influences the load-displacement curve, tensile strength, and rupture model. Zhou and Song [14] simulated and analyzed the influence of the size effect on the creep properties of rockfill; furthermore, the authors introduced a calculation equation that considers the size effect and stress level.

Limestone is often used for subgrade filling and dam construction. In the filler, limestone particles are often too large to test their mechanical properties in laboratory tests. It is difficult to investigate their macroscopic mechanical and deformation characteristics by means of laboratory tests. Filler compositions were usually downsized before laboratory tests, for which the strength and deformation parameters obtained in laboratory tests appear with a pronounced size effect due to the limits of sample size [15]. Li and Chen [16] revealed that the shear strength of intensively weathered granite decreases with increasing sample size. In the single-particle compression tests conducted by Zhou et al. [17], a numerical simulation of the single-particle compression test was performed, and the results indicated that the crushing strength of different particle groups follows the Weibull distribution and that the particle characteristic strength and particle size exhibit an exponential relationship. The sample is primarily formed by the mechanical disintegration of composition of the single particle. Xiao et al. [18, 19] showed that the strength and deformation behavior of rockfill materials are the key factors in determining the stability of the dam and are closely related to particle crushing characteristics. The particle size and shape of the single particle have an impact on particle strength. A single-particle compression test conducted by Meng et al. [20] showed that the particle crushing of mudstone and sandstone differs in the fractal dimension. As the minimum load-bearing unit of the rockfill, rock particles are vulnerable to crushing. Numerous studies have suggested that the strength of a single particle exhibits a noticeable size effect, which indicates that particle crushing strength decreases with increasing particle size. Dan et al. [21, 22] showed the spatial distribution of porosity is nonuniform, and permeability and porosity increase with time.

Laboratory tests, theoretical research, and numerical simulations have suggested that single-particle strength has a size effect. The size effect is influenced by the size, shape, and material of particles. Nevertheless, the influence of particle shapes on the size effect has not been studied extensively, which highlights the necessity of investigating this influence by quantifying the shapes of limestone particles.

In this study, we used a custom-designed particle shape measurement system to acquire digital images of limestone particles that were categorized into three particle groups, namely, 10–20 mm, 20–40 mm, and 40–60 mm. The particle profile was obtained using image processing software ImageJ, followed by particle shape parameter calculation. Subsequently, an analysis was performed based on shape quantification results. The influence of particle size features on the size effect of single-particle crushing strength was studied in combination with a single-particle compression test. The analysis results indicated that flatness and the axial coefficient decrease with increasing particle size. The results obtained herein would be beneficial to analyzing the size effect of particle strength.

2. Particle Contour Measurement Method

2.1. Materials. Limestone used in this study was collected from the rockfill of the Miaotang Dam, Wushan County, Chongqing. Limestone was ash-black carbonate rock, which is primarily composed of calcite with a small amount of dolomite. It was fresh and unweathered with a specific weight of 2.72 and a negligible water content of 0.05%. 100 particles were selected randomly for each particle group (10–20 mm, 20–40 mm, and 40–60 mm) for testing and analysis. Limestone particles are shown in Figure 1.

2.2. Particle Contour Capture Methods. To obtain the profiles of limestone particles, a 2D contour feature photography assistant system was produced based on the three-dimensional shape feature measurement system developed by Li et al. [23] for stone particles. It includes an outer frame, a light-transmitting plate, a wooden slat, a camera lever, and a light source, as shown in Figure 2. The particle image acquisition angle α was defined as the angle between the vertical direction of the camera and the light-transmitting plate. Five different acquisition angles ($\alpha = 30^{\circ}$, 60°, 90°, 120°, and 150°, 90° in Figure 2) were set by adjusting the placement of the light-transmitting plate and the wooden slat. To eliminate shadows during photography, the light source was placed under the light-transmitting plate. To mitigate the error caused by the distance between the camera and particles at different acquisition angles, the distance between the square holes in the outer frame was 600, 346, 173, 173, and 346, as shown in Figure 2.

The particle contour capture system requires the processing of numerical images into black and white binary images (or called as grayscale binary images) and threshold-based particle profile boundary distinction. The particle contour can be captured by the following steps: (1) digital image import, (2) image scale setting, (3) conversion into 8-bit grayscale images, (4) image binarization, (5) sharpening of the particle profile by threshold adjustment, (6) particle profile acquisition, and (7) shape parameter calculation. The particle contours of different acquisition angles are shown in Figure 3.

3. Particle Shape Classification and Shape Parameters

Particle shape plays a key role in determining particle grouping behavior. Accurate characterization and analysis of aggregate morphology are crucial for investigating particle material properties in more detail. Some researchers suggested making visual comparisons and describing particle shapes using charts [24–28]. First, Zingg [29] classified particle shapes into flat, spherical, foliated, and columnar based on the I/L and S/I ratios (L, I, and S represent the largest, second largest, and smallest sizes). Krumbein [30] developed a roundness comparison map. Powers [31] proposed a roundness scale for visual comparison and manual determination of roundness and sphericity. Krumbein and Sloss [32] suggested the estimation of particle shapes based on particle sphericity and roundness. Blott and Pye [33] furthered the findings of Zingg and developed a new chart based on the top quantile of I/L and S/I and used it to further classify particle shapes. A schematic of basic particle size parameters is shown in Figure 4, and the long and short axes of the equivalent ellipse were used.

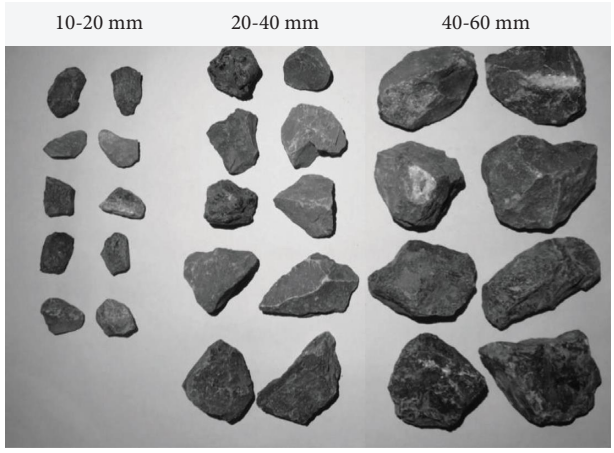

Figure 1: Limestone particles of different groups, 10–20 mm, 20–40 mm, and 40–60 mm.

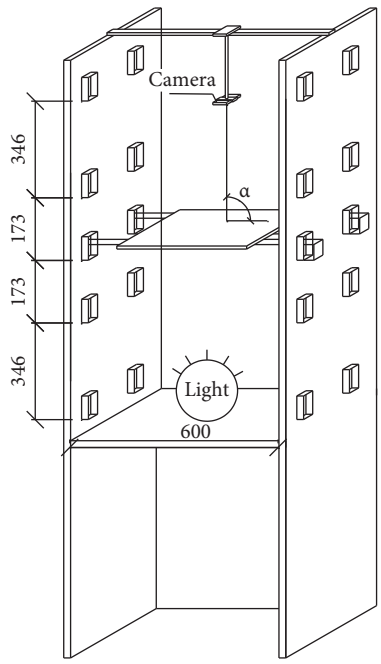

Figure 2: 2D contour feature photography assistant system.

Various methods are available for measuring L, I, and S [33]. Limestone particle size could be measured directly using a clipper or calculated by contours captured by using the 2D contour feature photography assistant system. L, I, and S represent three lengths in the orthogonal direction: I was perpendicular to L and S was perpendicular to L and I simultaneously. Therefore, the surface with the largest projection area (i.e., the surface where L and I are located) was placed as the bottom surface during image acquisition. S was measured at the surface perpendicular to L and I to obtain its top and front views, followed by L, I, and S calculations using ImageJ.

The particle shape can be described by three different characteristics. Macroscopically, particle shape features include flatness, overall profile coefficient, and roundness. Microscopically, the particle shape can be classified according to surface texture and roughness. Between macro and micro, the particle shape can be classified according to rounding degree and convexity. In this study, the particle shape was classified from the parameters listed in Table 1.

4. Particle Shape Classification Results and Discussion

In this study, the Simon shape classification method was used to classify limestone particles using the ratio relationships between I/L and S/I. Figure 5 shows the shape of classified limestone particles. Oblate, subspherical, and prolate particles accounted for a higher proportion in all particle groups, i.e., 90%, 87%, and 92% in the 10–20 mm, 20–40 mm, and 40–60 mm groups, respectively. Discoid or rod-shaped particles were scarce, and no spherical particles were present in the 40–60 mm group.

Table 2 shows the statistics of the shape parameters of the limestone particles in different particle size groups. The statistical average of each shape parameter was calculated based on 100 particles in each size group. The small variances of various shape parameters in each particle group indicated that parameters were less discrete. As shown in Figure 6, the statistical average of each shape parameter served as the ordinate and particle size served as the abscissa to investigate the variations in flatness, axial coefficient, roundness, sphericity, convexity, and roughness with particle size.

The larger the value of flatness e, the longer the particle. Larger flatness suggests a flatter, narrower, and longer particle. The closer e is to 1, the more spherical the overall particle shape. Figure 6 shows that with the increase in particle size, the flatness e and the axial coefficient aspect decreased, and the particle changed from elongated and flaky to subspherical.

Circularity R was used to characterize the degree of resemblance of the boundary of the particle plane to a circle. The closer it is to 1, the more circular the overall particle plane. Figure 6 shows that circularity R increased with particle size. Convexity C is used to characterize the angularity of a particle surface. The fewer the angles, the larger the convexity (≤ 1). As shown in Figure 6, convexity increased with particle size but at a smaller amplitude. This suggests that particle angularity decreases with increasing particle size.

Roughness r is a shape indicator used to describe the microscopic texture of the particle surface. The higher the roughness, the larger the fluctuation of the particle profile and the rougher the particle surface. As shown in Figure 6, roughness r showed an upward trend with the decrease in particle size, which indicates that the particle boundary becomes more irregular as particle size decreases.

5. Single-Particle Breakage Test

5.1. Test Method. Three hundred limestone particles were subjected to a single-particle compression test on a universal testing machine (Figure 7). An electrohydraulic servo control device with a maximum loading capacity of 500 kN was used with a loading rate of 1 mm/min. Before loading, the surfaces of limestone particles were cleaned by using a

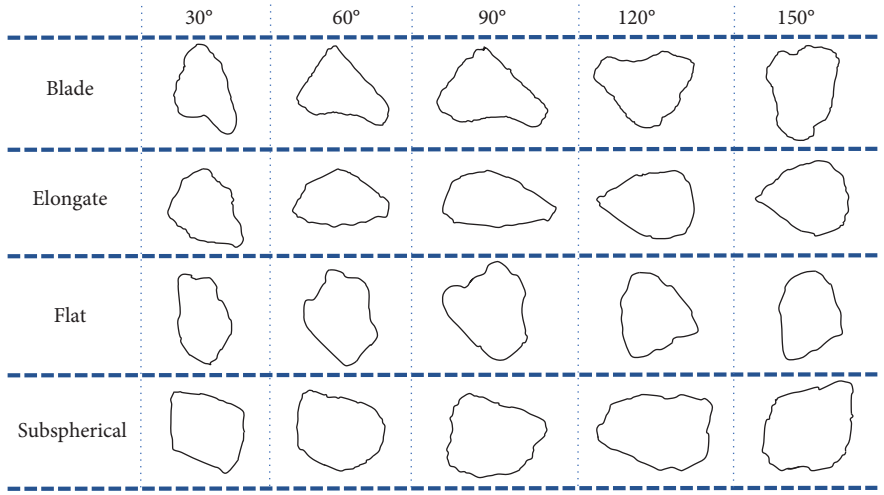

Figure 3: Particle contours of different acquisition angles.

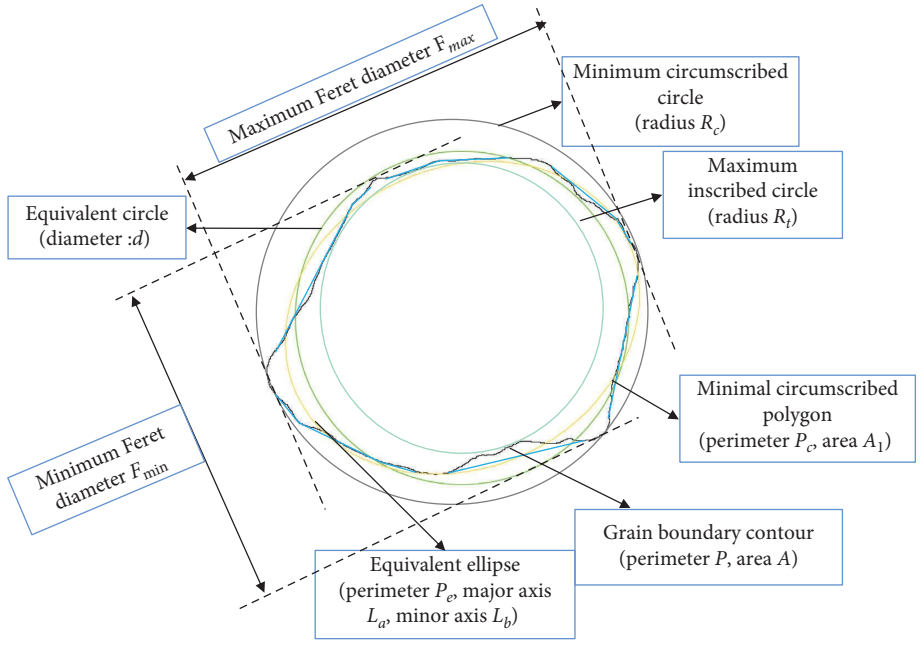

Figure 4: Schematic of basic particle size parameters.

Table 1: Particle shape parameters.

Level	Shape parameter	Formula	Basic size parameters
Describe the overall shape of the particle outline	Flatness: e Axial coefficient: aspect Circularity: R	$e = F_{max}/F_{min}$ Aspect $= L_a/L_b$ $R = 4\pi \times A/P^2$	F_{max} maximum Feret di ameter F_{min} minimum Feret diameter L_a equivalent ellipse major axis of contour projection L_b equivalent ellipse minor axis of contour projection P perimeter of contour projection A area of contour projection
Describe the angularity of particles	Convexity: C	$C = A/A_1$	A_1 smallest circumscribed polygonal area along the grain boundary
Describe the surface microtexture of structures	Roughness: r	$r = (P/P_C)^2$	P_C smallest circumscribed polygon perimeter along the grain boundary

brush, which were placed on upper and lower pressure plates. During the test, the surface where L and I were located was placed as the bottom surface for uniaxial compression. The upper loading plate was adjusted until it steadily contacted particles, and then start loading until the particle break. The test load and axial displacement data were

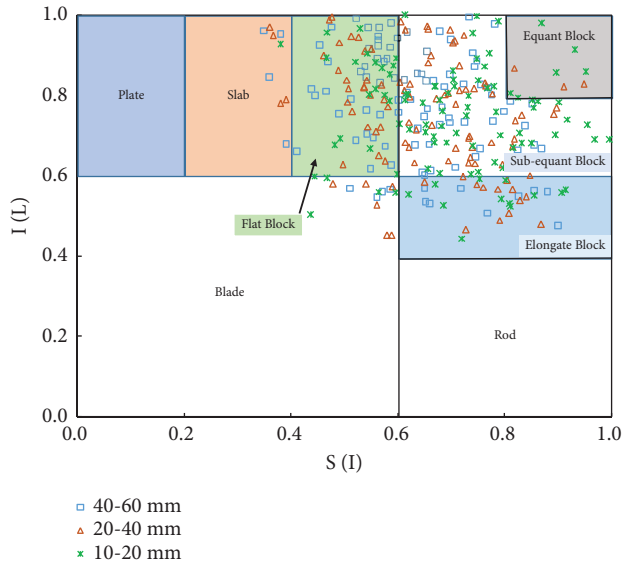

Figure 5: Simon shape classification diagram of limestone particles.

Table 2: Statistics of limestone particle shape parameters.

Grain size (mm)	Shape	Statistics			
		Average	Variance	Standard deviation	Coefficient of variation
10–20	*e*	1.44	0.03	0.17	0.11
	Aspect	1.42	0.03	0.18	0.13
	R	0.63	0.002	0.04	0.07
	C	0.95	0.001	0.03	0.04
	r	1.27	0.05	0.23	0.18
20–40	*e*	1.40	0.02	0.15	0.11
	Aspect	1.37	0.03	0.16	0.12
	R	0.75	0.001	0.04	0.05
	C	0.96	0.00	0.01	0.01
	r	1.21	0.001	0.04	0.03
40–60	*e*	1.38	0.02	0.13	0.09
	Aspect	1.35	0.02	0.14	0.10
	R	0.76	0.01	0.09	0.11
	C	0.97	0.00	0.01	0.01
	r	1.20	0.05	0.23	0.19

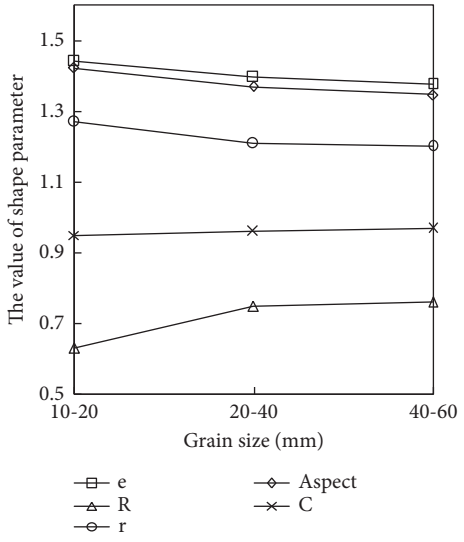

Figure 6: Variation of shape parameters with particle size.

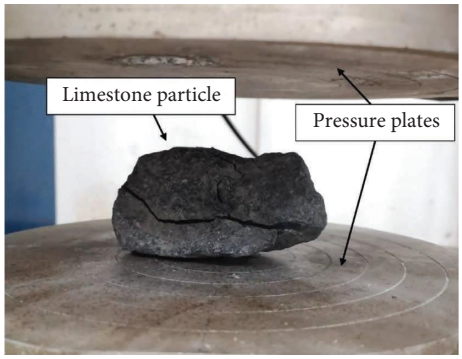

Figure 7: Universal tests.

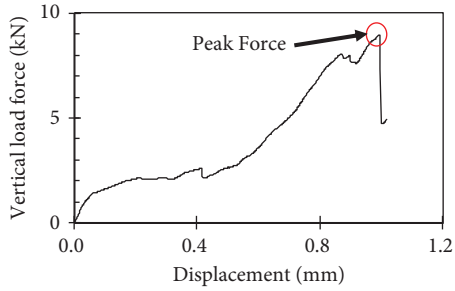

Figure 8: Typical force-displacement curve.

recorded by using the testing machine. Figure 8 shows the typical force-displacement curve. The point of the peak stress is shown in Figure 8.

5.2. Test Results. Figure 9 shows the scatterplot of the particle peak force and displacement. It can be seen that the test data points are scattered, and the peak load and its corresponding displacement in the same particle group are distributed over a wide range without an obvious pattern. The peak load force and displacement were the smallest in the 10–20 mm particle group; however, both increased and were distributed over a wider range with the increase in particle size. The peak load force and its corresponding displacement were particularly discrete in the 40–60 mm particle group. Furthermore, different particle groups overlapped with each other. Thus, a statistical method was used to analyze the crushing strength of limestone particles.

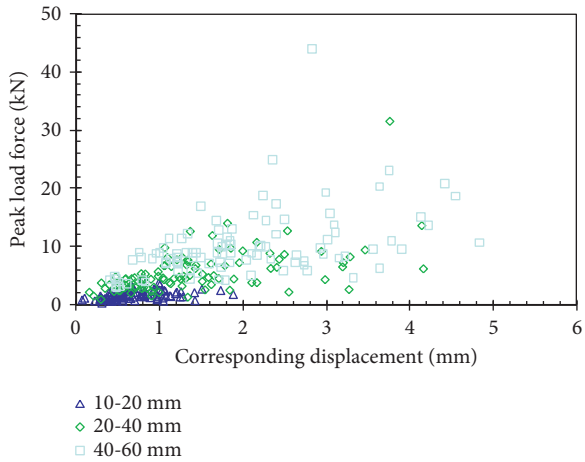

Figure 9: The valuation of the peak stress and displacement.

6. Discussion

6.1. Weibull Statistical Distribution. At present, researchers have performed compression tests for brittle materials with different particle shapes and calculated crushing strength by Equation (1), as shown in Table 3, implying that the equation is reasonable for nonspherical (or non-sub-spherical) shapes.

The tensile strength of rock or soil is usually measured indirectly by compressing the particles between plates until they fail. McDowell and Amon [34] defined the bursting stress (crushing strength σ) on a single particle with a diameter d under the action of force F as follows:

$$\sigma = \frac{F}{d^2}, \tag{1}$$

where F is the peak load force upon particle crushing (N), d is the distance between the upper and lower loading plates, which is also the nominal particle diameter (mm), and σ is the bursting stress on the particle (MPa).

Previous research indicates that particle crushing strength follows the Weibull distribution. Based on the Weibull weakest link theory, McDowell and Amon [34] described the survival probability ($P_s(d)$) of a particle with a diameter d loaded between plates as follows:

$$P_s(d) = \exp\left[-\left(\frac{d}{d_0}\right)^3\left(\frac{\sigma}{\sigma_0}\right)^m\right], \tag{2}$$

where d_0 is the reference particle size (mm), σ_0 is the characteristic stress at a particle survival probability of 37% (MPa), and m is the Weibull modulus, which decreases with the increase in strength discreteness. Strength discreteness determines the size effect of strength.

From Equation (2), the strength relationship of different particle sizes of the same granular material can be deduced as follows:

$$P_S(d_a) = \exp\left(-\left(\frac{d_a}{d_a^0}\right)^3\left(\frac{\sigma_a}{\sigma_a^0}\right)^{m_a}\right). \tag{3}$$

$$P_S(d_b) = \exp\left(-\left(\frac{d_b}{d_b^0}\right)^3\left(\frac{\sigma_b}{\sigma_b^0}\right)^{m_b}\right). \tag{4}$$

Since particle materials were the same, the following equation can be obtained:

$$d_a^0 = d_b^0, \sigma_a^0 = \sigma_b^0, m_a = m_b. \tag{5}$$

The correlation between the characteristic stress and particle size can be derived as follows:

Table 3: Test results of different particle materials.

Number	Author	Material	Particle shape	Crushing strength (MPa)
[1]	Stefanou and Sulem	Rock sugar grain	Realistic grain shape (3 mm < d < 5 mm)	3.76
[2]	Yu et al.	Glass	Angular (0.85 mm < d < 1 mm)	62.1
[3]	Ham et al.	Quartz dry	Angular (1.1 mm < d < 2.0 mm)	23.3
[4]	Koohmishi and Palassi	Ballast	Quasi-spherical (10 mm < d < 14 mm)	37.8
		Basalt	Hexahedron (50 mm < d < 62.5 mm)	9.14
		Marl	Pentahedron (50 mm < d < 62.5 mm)	6.2
		Dolomite	Tetrahedron (50 mm < d < 62.5 mm)	16.89
[5]	Lobo-Guerrero and Vallejo	Biotite gneiss	Angular (4 mm < d < 10 mm)	23.56
[6]	Ovalle et al.	Calcareous rock	Angular (7 mm < d < 15 mm)	3.35

$$\sigma_0 \propto d^{-\frac{3}{m}}. \tag{6}$$

The cumulative survival probability of particles in a certain particle group [35] is given by

$$P_s(\sigma) = 1 - \frac{i}{n+1}, \tag{7}$$

where n is the total number of test samples, according to the single-particle strength of the samples in ascending order. Given that the single grain strength of the sample at a position i in the sequence is σ_i, the probability that the grain-sized sample is not broken under a certain stress is $P_s(\sigma)$.

For particles of the same size, $d = d_0$. By substituting this equation into Equation (2) and taking logarithm on both sides, the following equation is obtained:

$$\ln\left[\ln\left(\frac{1}{P_s}\right)\right] = m \ln \frac{\sigma}{\sigma_0}. \tag{8}$$

It can be inferred that ln (ln $(1/P_s)$) and lnσ are linearly related. The Weibull modulus (m) is the slope of the straight line, and the characteristic stress (σ_0) can be obtained based on the intercept of the straight line on the x-axis. Considering that the strength of single particles in a rockfill with the same particle size is discrete, the single-particle strength of the rockfill within a certain range of particle sizes is typically characterized by the characteristic stress (σ_0) [36].

The crushing strengths of the 100 particles in each of the three particle groups are plotted in Figure 10. Based on the particle strength fitting curves of various particle groups shown in Figure 10 and Equation (8), the Weibull parameters of the single-particle strength distributions of different particle groups were obtained (Table 4).

Figure 10 shows that the particle crushing stress of the three size group particles can be plotted by following the Weibull distribution, except for ln(σ) lower than 1.42, 1.47, and 1.54 for 40–60 mm, 20–40 mm, and 10–20 mm particle groups, respectively. The values of the Weibull parameter m were 2.82, 2.87, and 2.76 for 40–60 mm, 20–40 mm, and 10–20 mm particle groups, respectively. The average of m *is* 2.82. The characteristic stresses of 40–60 mm, 20–40 mm, and 10–20 mm particle groups were 9.346, 13.176, and 14.59 MPa, respectively. The characteristic stress increased with the decrease in particle size, suggesting that the crushing stress of limestone particles is closely related to particle size.

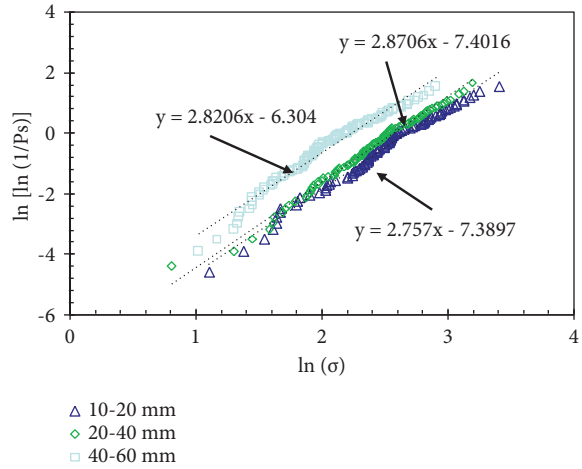

Figure 10: Weibull distribution diagram of particle crushing strength.

Table 4: Granular crushing strength of Weibull distribution parameters.

Grain size (mm)	M	σ_0 (MPa)	R^2
10–20	2.76	14.59	0.99
20–40	2.87	13.18	0.98
40–60	2.82	9.35	0.97

6.2. Influence of Particle Shape on the Size Effect of Particle Strength. To investigate the relationship between particle shape and particle crushing strength, the Weibull distribution of particle crushing intensity for bladed, long spherical, flat spherical, and subspherical particles is plotted in Figure 11. Based on the crushing strength fitting curve of each particle group and Equation (8) as shown in Figure 11, the corresponding parameters Weibull moduli (m) and characteristic stresses (σ_0) were obtained, as shown in Table 5. Table 5 shows that when the particle shape is the same, m basically remains the same as the particle size increases and σ_0 gradually decreases. The Weibull moduli (m) of particles with different shapes were in the following ascending order: blade particles < elongated particles < flat particles < subspherical particles. This indicates that the more irregular the particle shape, the smaller the Weibull modulus (m) and the more discrete the particle crushing strength. A higher particle shape irregularity indicates a more complex stress state and stronger discreteness of

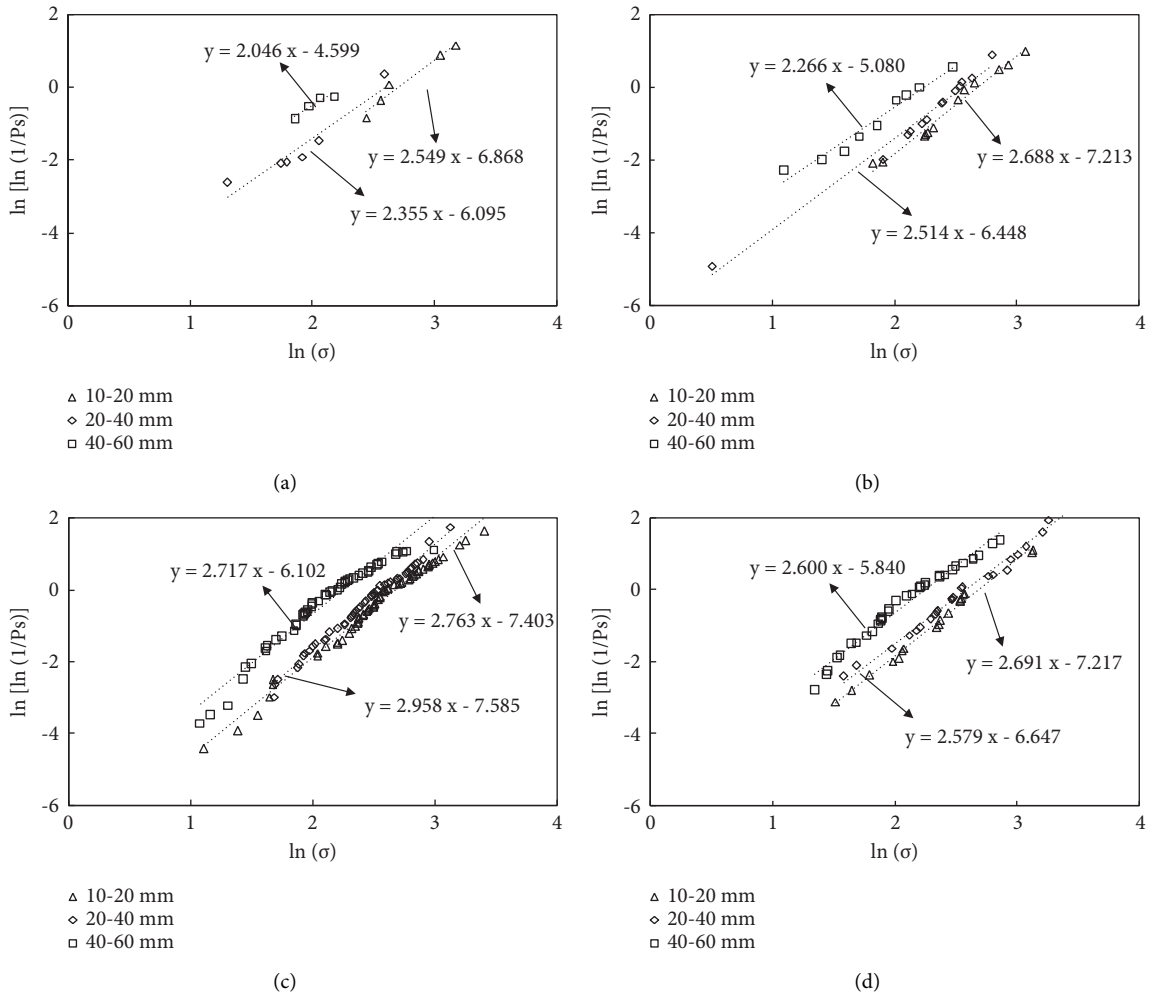

Figure 11: Weibull distribution diagram of crushing strength of four types of particles: (a) foliated particles, (b) elongated particles, (c) subspherical particles, and (d) flat particles.

Table 5: Weibull parameter of crushing strength of particles with four different shapes.

Grain size (mm)	Parameters	Blade particles	Elongated particles	Flat particles	Subspherical particles
10–20	m	2.55	2.69	2.69	2.76
	σ_0 (MPa)	14.79	14.64	14.61	14.58
20–40	M	2.36	2.51	2.58	2.96
	σ_0 (MPa)	13.31	13.00	13.16	12.99
40–60	M	2.05	2.27	2.60	2.72
	σ_0 (MPa)	9.46	9.41	9.45	9.45

particle crushing strength. When the shape of particles is closer to a circle, the characteristic stress intensities of particles of the same size are closer. In general, the characteristic stress decreases significantly as particle morphology changes from small-sized blade to large-sized subspherical, while the Weibull modulus remains essentially unchanged.

The relationship between the characteristic stress (σ_0) and particle size of particles with four different shapes is plotted in Figure 12. As shown in Figure 12, the characteristic stress (σ_0) of particles with the same shape decreased with increasing particle size, indicating that particle crushing strength has a size effect. A power function was used to fit the relationship between the characteristic stress (σ_0) and particle size of particles with four different shapes, with the power indexes listed in Table 6.

Table 6 shows that Equation (3) presents the relationship between the characteristic stress (σ_0) and particle size of particles, where the power index of foliated particles is $-3/m = -3/2.317 = -1.30$; the mean of the Weibull modulus (m) of foliated particles was determined based on Table 5. As shown in Table 6, the power indexes obtained by calculation and those obtained by fitting differed significantly from each other. Lim et al. [37] expounded on the reason that the size

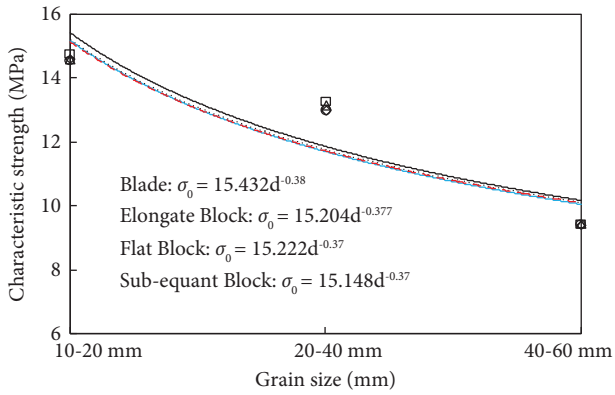

Figure 12: Relationship between the characteristic stress and particle size function of four types of particle shapes.

Table 6: Power function parameters within four different shapes.

Shape	Value	
	$-3/m$ by fitting	Value m by Equation (3)
Blade particles	−0.38	−1.30
Elongated particles	−0.38	−1.21
Flat particles	−0.37	−1.14
Subspherical particles	−0.37	−1.07

effect of particle materials is weaker than that predicted by the Weibull model. McDowell and Amon [34] derived a size effect by assuming that the material was homogeneous and anisotropic. However, particles of different sizes differed in their internal structure, leading to larger errors in the Weibull statistical analysis of the size effect of particle breaking strength.

Although the power index and Weibull modulus (m) did not strictly follow the $-3/m$ relationship when the size effect was predicted using the Weibull model, the positive correlation was obvious between the Weibull modulus (m) and the power index. A comparison of the power indexes of particles with four different shapes (Table 6) indicates that the more irregular the particles, the smaller the Weibull modulus (m), the smaller the power index, and the more prominent the size effect of particle strength.

In addition, Figure 12 plots that the relationship between the characteristic stress (σ_0) and particle size may not be the power function. It seems there is a quadratic function between the characteristic stress (σ_0) and particle size. In future studies, the relationship between the characteristic stress and particle size under different particle shapes should be carried out.

7. Conclusion

(1) 90 percent of limestone particle shapes were oblate spherical, subspherical, and long spherical particles randomly selected from the soil foundation.

(2) The characteristic stress of limestone particles increased with increased particle size. The crushing strength of limestone particles increased with the increase in particle size. The relationship between the characteristic strength and particle size can be fitted by a power exponential formulation of four types of limestone particle shapes.

(3) The more irregular the particle shape, the smaller the Weibull modulus (m) and power index and the more obvious the particle strength size effect. The relationship between the characteristic stress (σ_0) and particle size was a power function. The values of the parameters of the function depend on the particle size and the relationship between the characteristic stress (σ_0).

Data Availability

The data used to support the findings of this study are available from the corresponding author upon request.

Conflicts of Interest

The authors declare that they have no conflicts of interest.

Acknowledgments

The authors gratefully acknowledge financial support from the National Natural Science Foundation of China-Yalong River Basin Hydropower Development Co., Ltd., Yalong River Joint Fund under grant no. U1865103, the Chongqing Municipal Construction Committee Science and Technology Plan Project Grant No. 2022-1-15, the Science and Technology Research Program of Chongqing Municipal Education Commission Grant No. KJQN202000747 and KJZD-K202000705, the China Postdoctoral Science Foundation funded project grant No. 2019M663890XB, the Chongqing Postdoctoral Science Foundation funded project grant no. 228512. The authors would like to thank Editage (https://www.editage.cn/) for English language editing.

References

[1] R. M. Koerner, "Effect of particle characteristics on soil strength," *Journal of the Soil Mechanics and Foundations Division*, vol. 96, no. 4, pp. 1221–1234, 1970.

[2] K. Miura, K. Maeda, M. Furukawa, and S. Toki, "Mechanical characteristics of sands with different primary properties," *Soils and Foundations*, vol. 38, no. 4, pp. 159–172, 1998.

[3] K. A. Alshibli and M. I. Alsaleh, "Characterizing surface roughness and shape of sands using digital microscopy," *Journal of Computing in Civil Engineering*, vol. 18, no. 1, pp. 36–45, 2004.

[4] G.-C. Cho, J. Dodds, and J. C. Santamarina, "Particle shape effects on packing density, stiffness, and strength: Natural and crushed sands," *Journal of Geotechnical and Geoenvironmental Engineering*, vol. 132, no. 5, pp. 591–602, 2006.

[5] P. Guo and X. Su, "Shear strength, interparticle locking, and dilatancy of granular materials," *Canadian Geotechnical Journal*, vol. 44, no. 5, pp. 579–591, 2007.

[6] R. H. Brzesowsky, C. J. Spiers, C. J. Peach, and S. J. T. Hangx, "Failure behavior of single sand grains: theory versus experiment," *Journal of Geophysical Research*, vol. 116, no. B6, pp. B06205–B7121, 2011.

[7] E. Frossard, W. Hu, C. Dano, and P. Y. Hicher, "Rockfill shear strength evaluation: a rational method based on size effects," *Géotechnique*, vol. 62, no. 5, pp. 415–427, 2012.

[8] K. J. Wang, Y. F. Jia, and S. C. Chi, "Study on broken characteristics of rockfill materials based on single particle compression test," *Yangtze River*, vol. 51, no. 03, pp. 160–166, 2020.

[9] J. Huang, S. Xu, H. Yi, and S. Hu, "Size effect on the compression breakage strengths of glass particles," *Powder Technology*, vol. 268, pp. 86–94, 2014.

[10] Y. F. Xu, Y. D. Wang, Y. Xi, and C Feifei, "Size effect on crushing of rock particles," *Journal of Engineering Geology*, vol. 22, no. 06, pp. 1023–1027, 2014.

[11] X. F. Mi and S. C. Chi, "Size effects of rockfill particle strength," *Journal of Water Resources and Architectural Engineering*, vol. 17, no. 04, p. 182, 2019.

[12] X. Li, G. Ma, W. Zhou et al., "Scale effects of rockfill materials considering size effect of particle strength," *Journal of Hydroelectric Engineering*, vol. 35, no. 12, pp. 12–22, 2016.

[13] Y. H. Huang, S. Q. Yang, Y. Ju, X. P. Zhou, and J. Zhou, "Study on particle size effects on strength and crack coalescence behavior of rock during Brazilian splitting test," *Journal of Central South University*, vol. 47, no. 04, pp. 1272–1281, 2016.

[14] M. J. Zhou and E. X. Song, "A random virtual crack dem model for creep behavior of rockfill based on the subcritical crack propagation theory," *Acta Geotechnica*, vol. 11, no. 4, pp. 827–847, 2016.

[15] E. J. Garboczi, K. A. Riding, and M. Mirzahosseini, "Particle shape effects on particle size measurement for crushed waste glass," *Advanced Powder Technology*, vol. 28, no. 2, pp. 648–657, 2017.

[16] C. Y. Li and Z. B. Chen, "Specimen size effect of strongly weathered granite of seabed in triaxial tests under K0-consolidation condition," *Journal of Central South University*, vol. 51, no. 06, pp. 1646–1653, 2020.

[17] H. J. Zhou, G. Ma, W. Yuan, and Z Wei, "Size effect on the crushing strengths of rock particles," *Rock and Soil Mechanics*, vol. 38, no. 8, pp. 2425–2433, 2017.

[18] Y. Xiao, L. Long, T. Matthew Evans, H. Zhou, H. Liu, and A. W. Stuedlein, "Effect of particle shape on stress-dilatancy responses of medium-dense sands," *Journal of Geotechnical and Geoenvironmental Engineering*, vol. 145, no. 2, Article ID 04018105, 2019.

[19] Y. Xiao, M. Q. Meng, A. Daouadji, Q. Chen, Z. Wu, and X. Jiang, "Effects of particle size on crushing and deformation behaviors of rockfill materials," *Geoscience Frontiers*, vol. 11, no. 2, pp. 375–388, 2020.

[20] M. Q. Meng, L. Wang, X. Jiang, and G Cheng, "Single-particle crushing test and numerical simulation of coarse grained soil based on size effect," *Rock and Soil Mechanics*, vol. 41, no. 09, pp. 2953–2962, 2020.

[21] M. Dan, J. Zhang, H. Duan et al., "Reutilization of gangue wastes in underground backfilling mining: overburden aquifer protection," *Chemosphere*, vol. 264, Article ID 128400, 2021.

[22] M. Dan, H. Duan, and J. Zhang, "Solid grain migration on hydraulic properties of fault rocks in underground mining tunnel: radial seepage experiments and verification of permeability prediction," *Tunnelling and Underground Space Technology*, vol. 126, Article ID 104525, 2022.

[23] R. Z. Li, W. B. Lu, Y. J. Yi, and Y. J. Yu, "Study on the shape and specific surface area characteristics of blasting gravel particles of Limestone in the Hangudi quarry of Baihetan," *Chinese Journal of Rock Mechanics andEngineering*, vol. 38, no. 7, pp. 1344–1354, 2019.

[24] C. X. Lin, S. Y. Zhong, and S. D. Ling, "Analysis of particle shape characteristics of lunar soil simulant and its effect on shear strength," *Journal of Northeastern University*, vol. 37, no. 11, pp. 1640–1644, 2016.

[25] Y. H. Yang, Z. A. Wei, Y. L. Chen, and B. X. Ren, "REN Bingxu. Study on the shapes of tailings particles based on microscopy and image processing technologies," *Chinese Journal of Rock Mechanics and Engineering*, vol. 36, no. Supp.1, pp. 3689–3695, 2017.

[26] X. B. Tu and S. J. Wang, "Particle shape descriptor in digital image analysis[J]," *Chinese Journal of Geotechnical Engineering*, vol. 26, no. 5, pp. 659–662, 2004.

[27] Q. B. Liu, W. Xiang, M. Budbu, and D. S. Cui, "Study of particle shape quantification and effect on mechanical property of sand," *Rock and Soil Mechanics*, vol. 32, no. Supp.1, pp. 190–197, 2011.

[28] D. G. Zou, J. R. Tian, J. M. Liu, and C Zhou, "Three-dimensional shape of rockfill material and its influence on particle breakage," *Rock and Soil Mechanics*, vol. 39, no. 10, pp. 3525–3530, 2018.

[29] T. Zingg, "Beitrag zur schotteranalyse," *Schweizerische Mineralogische Und Petrographische Mitteilungen*, vol. 15, pp. 39–140, 1935.

[30] W. C. Krumbein, "Measurement and geological significance of shape and roundness of sedimentary particles," *Journal of Sedimentary Research*, vol. 11, pp. 64–72, 1941.

[31] M. C. Powers, "A new roundness scale for sedimentary particles," *SEPM J Sediment Res*, vol. 23, pp. 117–119, 1953.

[32] W. C. Krumbein and L. L. Sloss, *Stratigraphy and Sedimentation*, W.H. Freeman and Company, San Francisco, CA, USA, Second Edi edition, 1963.

[33] S J. Blott and K. Pye, "Particle shape: a review and new methods of characterization and classification," *Sedimentology*, vol. 55, no. 1, pp. 31–63, 2010.

[34] G. R. Mcdowell and A. Amon, "The application of Weibull statistics to the fracture of soil particles," *Soils and Foundations*, vol. 40, no. 5, pp. 133–141, 2000.

[35] L. I. Yang and C. She, "Numerical simulation of effect of size on crushing strength of rockfill grains using particle flow code," *Rock and Soil Mechanics*, vol. 39, no. 08, pp. 2951–2959+2976, 2018.

[36] S. C. Chi, F. Wang, and Y. F. Jia, "Modeling particle breakage of rockfill materials based on single particle strength," *Chinese Journal of Geotechnical Engineering*, vol. 37, no. 10, pp. 1780–1785, 2015.

[37] W. L. Lim, G. R. Mcdowell, and A. C. Collop, "The application of Weibull statistics to the strength of railway ballast," *Granular Matter*, vol. 6, no. 4, pp. 229–237, 2004.

[38] Z. Z. Sun, G. Ma, and W. Zhou, "Effect of particle shape on size effect of crushing strength of rockfill particles," *Rock and Soil Mechanics*, vol. 42, no. 02, pp. 430–438, 2021.

[39] J. F. Zhang, J. B. Ye, J. S. Chen, and L SL, "A preliminary study of measurement and evaluation of breakstone grain shape," *Rock and Soil Mechanics*, vol. 37, no. 2, pp. 343–349, 2016.